



# End-to-End Error Control Coding Capability of NB-IoT Transmissions in a GEO Satellite System with Time-Packed Optical Feeder Link

Joan Bas<sup>1(✉)</sup> and Alexis A. Dowhuszko<sup>2</sup>

<sup>1</sup> Department of Array & Multi-Sensor Processing, Centre Tecnològic de Telecomunicacions de Catalunya (CTTC), Castelldefels, Spain

joan.bas@cttc.es

<sup>2</sup> Department of Communications and Networking, Aalto University, Espoo, Finland

alexis.dowhuszko@aalto.fi

**Abstract.** This paper focuses on the return link of a GEO satellite system that collects information from a large number of sparsely distributed IoT devices in a large geographical area. Narrow-Band (NB) IoT transmissions, with suitable Modulation and Coding Scheme (MCS), are Detected-and-Forwarded onboard the satellite, mapping each QAM symbol of the radio access link (uplink) into another PAM symbol that modulates optical feeder link's intensity (downlink). Given the massive number of IoT devices that is expected to be served by the GEO satellite system, the feeder link (downlink) of the return channel is expected to be the bottleneck. To tackle this limitation, time-packing signaling is used in the waveform that modulates the intensity of the optical feeder link (downlink); this way, the symbol time is reduced, and the number of IoT devices that can be simultaneously served in the radio access link (uplink) can augment without increasing the signal bandwidth in the optical feeder link. The Inter-Symbol Interference (ISI) that the time-packed feeder link generates is partially mitigated in the satellite gateway, using for this purpose an adaptive linear equalizer. After optical-to-electrical conversion, the NB-IoT codewords that are received in the gateway are decoded, correcting simultaneously errors introduced in both radio access and optical feeder links. The aim of this paper is to evaluate the error correction capability that MCS of NB-IoT standard has when used to protect end-to-end the hybrid radio/optical return link that results, particularly when using large overlapping factors in the optical feeder link to increase its achievable data rate.

**Keywords:** High-Throughput Satellite · Optical feeder link · Narrow-Band IoT · Return channel · Time-packing · Modulation and coding

This work has received funding from the Spanish Ministry of Science, Innovation and Universities under project TERESA-TEC2017-90093-C3-1-R (AEI/FEDER, UE) and from the Catalan Government under grants 2017-SGR-891 and 2017-SGR-1479.

## 1 Introduction

The improvement of spectral efficiency is key for achieving higher data rate links in the next generation of wireless communication systems. This fact becomes critical in Satellite Communications (SatCom) and IoT systems, where the link propagation delay is large and the orders of the modulation schemes that are available for communication are low. In this regard, the Faster-Than-Nyquist (FTN) technique [12], so-called *time-packing*, has been recently reconsidered as a good candidate solution for increasing the spectral efficiency of Beyond 5G [14]. As a side-benefit, time-packing can also provide some additional PHY-layer security feature by adjusting the temporal separation between consecutive pulse-shapes, such that only the authorized user(s) is(are) able to detect the transmitted symbol stream with low enough Bit Error Rate (BER) [6].

The increased spectral efficiency that time-packing provides, as well as the additional PHY-layer security feature that enables, represents an interesting combination that would fuel the commercial success Satellite-based IoT services. According to Northern Sky Research reports, telemetry applications have the largest share (28%) when measuring the services with highest economic impact in IoT technology nowadays, followed by Telematics/Analytics applications (13%) and Asset Tracking services (11%), respectively [11, 15]. It is important to highlight that the three previously listed IoT applications usually demand Narrow-Band (NB) communications and high levels of security. Therefore, time-packing is a good candidate solution to fulfill these two IoT requirements, particularly when relying on SatCom systems with extremely large coverage areas.

The use of time-packing reduces the temporal duration of the IoT frames, which is beneficial for increasing the amount of traffic that can be simultaneously collected in the radio access links – enabled by multiple spot-beams, which is then aggregated in the point-to-point optical feeder link toward the satellite gateway. However, the use of time-packing in optical feeder links has also some implementation challenges. For example, when adjacent data-carrying pulses are more densely packed in time, the Peak-to-Average Power Ratio (PAPR) of the resulting time-domain signal increases, reducing the end-to-end spectral efficiency as certain blocks of the transmission chain – such as the radio power amplifiers and the external optical Match-Zehnder Modulators (MZM) – have a linear response only on a limited input signal range. It is important to highlight that the PAPR of the time-packed waveform does not depend only on the selected overlapping factor, but also on the roll-off factor of the pulse-shaping filter that is used, which could be *e.g.* a Square-Root Raised-Cosine (SRRC) filter [5].

Finally, when focusing on the received signal processing in the satellite gateway, we note that the use of large overlapping factors and/or low roll-off factors on the time-packed waveform introduces notable Inter-Symbol Interference (ISI). This means that it is very difficult to implement a Maximum Likelihood Sequence Detector (MLSD) or Viterbi Equalizer, particularly when the modulation order of the data-carrying signal is large. Therefore, sub-optimal adaptive linear equalizers can be used to remove most of the ISI that time-packing introduces and,

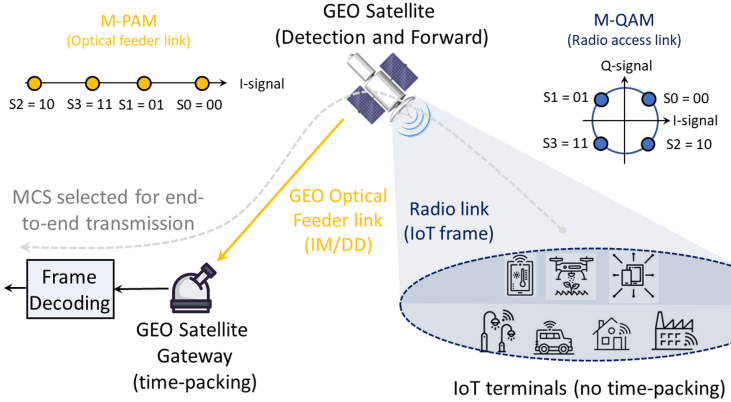


**Fig. 1.** Block diagram of a GEO satellite system that implements time-packing in the optical feeder link to augment the number of connected NB-IoT devices that can be simultaneously served. The GEO satellite implements a Detection-and-Forward strategy, mapping the  $M$ -QAM symbols of the radio access link to  $M$ -PAM symbols to modulate the intensity of the laser diode. The coding scheme that the NB-IoT devices select is used to correct errors introduced in both radio access and optical feeder parts of the return link.

after that, a low-complexity symbol-by-symbol detectors can be implemented. In this paper, we aim at characterizing the end-to-end error control correction capabilities that Modulation and Coding Schemes (MCS) of NB-IoT standard can provide when concatenating the radio access link with the optical feeder link in a GEO SatCom system. Note that the use of end-to-end error control coding makes sense in low-complexity satellite systems, as no additional decoding/encoding processing is needed onboard the satellite to protect the end-to-end transmission against the error in the optical part. This is the reason why the Detection-and-Forward architecture has been proposed, where only the hard-detection of the  $M$ -QAM symbols (access link) and its mapping into  $M$ -PAM symbols (feeder link) should be performed onboard the satellite.

This paper has been structured as follows: Sect. 2 presents the system model, including details of the NB-IoT transmission on the radio access link, as well as the generation of the time-packed signal that modulates the intensity of the optical feeder link. Section 3 explains the adaptive linear equalization approach that is used to mitigate the ISI that time-packing generates, whereas Sect. 4 presents the simulation setup and the performance evaluation when different MCS of NB-IoT standard are used to control the errors introduced end-to-end in the reverse. Finally, Sect. 5 summarizes the main outcomes.

## 2 System Model

The block diagram of the proposed High-Throughput Satellite (HTS) system model is shown in Fig. 1. It consists of a large number of sparsely deployed

**Table 1.** Details of the Resource Units and Uplink slots for each NPUSCH format, including separations between different subcarriers (see Table 10.1.2.3-1 of [2]).

NPUSCH format	$\Delta f$	$N_{sc}^{RU}$	$N_{slots}^{UL}$	$N_{symbol}^{UL}$
1	3.75 kHz	1	16	7
		1	16	
	15 kHz	3	8	
		6	4	
		12	2	
2	3.75 kHz	1	4	
	15 kHz	1	4	

IoT devices, which use the Geosynchronous Equatorial Orbit (GEO) satellite as Detect-and-Forward relaying node to reach the remote satellite gateway. Different wireless communication technologies are used for the access link (uplink) and feeder link (downlink), namely radio and optical wireless, respectively.

The radio waveform that the IoT terminals generate for the uplink transmission follows the NB-IoT standard. In the satellite, the  $M$ -QAM symbols that are received in uplink are first detected and then mapped into points of an  $M$ -PAM constellation, to make them suitable to modulate in intensity the light beam that the laser diode on-board the satellite emits in downlink. When performing this electrical-to-optical conversion, the time-packing feature is introduced in the  $M$ -PAM downlink transmission to reduce the symbol time and increase the number of IoT terminals that can be simultaneously served in the satellite spot-beams. In the next sections, the signal model for both radio access link and optical feeder link are explained in further detail.

## 2.1 NB-IoT Transmission in Radio Access (Uplink of Reverse Link)

The reverse NB-IoT communication, which starts in the IoT device(s) and ends in the satellite gateway, consist of the following physical channels [1–3]:

- Narrowband Physical Uplink Shared Channel (NPUSCH), which is used to transmit uplink transport block on the orthogonal Resource Units (RUs) that have been scheduled for the target IoT device.
- Narrow Band Physical Random Access Channels (NPRACH), which enables the random access procedure among the IoT devices that have information to transmit in the shared radio access link.

From both channels, this paper focused on the NPUSCH, and assumes that the random access procedure has been successfully performed, such that the IoT devices known the orthogonal RUs that have been reserved for its uplink communication. The NPUSCH is based on the following parts: 24 bits of Cyclic Redundancy Check (CRC), Turbo channel encoding with a mother code of 1/3, rate matching, physical-layer Hybrid Automatic Repeat Request (HARQ), scrambling, modulations of  $\pi/2$ -BPSK and  $\pi/4$ -QPSK for single-tone transmissions, and QPSK for multi-tone transmissions.

**Table 2.** Supported modulation formats in NPUSCH (see Table 10.1.3.2-1 of [2]).

NPUSCH format	$N_{sc}^{RU}$	Modulation scheme
1	1	BPSK, QPSK
	>1	QPSK
2	1	BPSK

**Table 3.** Relation/mapping between Modulation order, Transport Block Size index, and Modulation and Coding Scheme index (see Table 16.5.1.2-1 of [3]).

MCS Index $I_{MCS}$	Modulation Order $Q_m$	TBS Index $I_{TBS}$
0	1	0
1	1	2
2	2	1
3	2	3
4	2	4
5	2	5
6	2	6
7	2	7
8	2	8
9	2	9
10	2	10

Moreover, the NPUSCH has two formats: Format 1 is used for data transmissions on the Uplink Shared Channel (UL-SCH), whereas Format 2 is used for Uplink Control Information (UCI), such as ACK/NACK transmissions of the HARQ mechanism. The uplink transmission can support two different sub-carrier separations ( $\Delta f$ ). When  $\Delta f = 15$  kHz, 12 consecutive sub-carriers are allocated for uplink transmission using time slots of duration 0.5 ms. On the other hand, when  $\Delta f = 3.75$  kHz, 48 consecutive sub-carriers are allocated for uplink transmission in time slots of duration 2 ms. The distribution of the number of resource units ( $N_{sc}^{RU}$ ) and number of slots ( $N_{slots}^{UL}$ ) for the different formats of the NPUSCH is provided in Table 1 (See Table 10.1.2.3-1 of [2]). The modulation scheme that is used depends on the value that  $N_{sc}^{RU}$  takes, as illustrated in Table 2 (See Table 10.1.3.2-1 of [2]). From this table, we will focus on Format 1 and single-subcarrier transmissions (*i.e.*,  $N_{sc}^{RU} = 1$ ), since it enables the use of both BPSK and QPSK modulation schemes.

The following step consists in associating the modulation format with the error control coding scheme, which will define the Transport Block Size (TBS) and the corresponding code rate. More precisely, the NPUSCH can support up to 11 different MCS, whose relation with the modulation and TBS index is shown in Table 3 (See Table 16.5.1.2-1 of [3]). From these values, we observe that BPSK modulation is used only in the first two possible MCS indexes (*i.e.*,  $I_{MCS} = 0, 1$ ), whereas the other MCS indexes rely on QPSK modulation (*i.e.*,  $I_{MCS} = 2, \dots, 10$ ). Table 3 also relates the index of the MCS ( $I_{MCS}$ ) with the index of the TBS ( $I_{TBS}$ ). NB-IoT has multiple possible TBS values, which depend on

the modulation and the code rate that is used in each case. Thus, from the  $I_{\text{TBS}}$  point of view, the first and third MCS indexes utilize BPSK, whereas the others utilize QPSK. Then, in order to identify the transport block size, Table 4 associates each TBS index ( $I_{\text{TBS}}$ ) with the Resource Unit index ( $I_{\text{RU}}$ ).

From Table 4, it is possible to observe that the minimum and maximum TBS for the NPUSCH is 16 bits and 2536 bits, respectively. We note that the different TBS may be associated with different modulation formats. For example, when BPSK modulation is used, the minimum and maximum TBS that is possible is 16 bits and 424 bits, respectively. On the other hand, when using QPSK modulation, the minimum and maximum TBS is 24 bits and 2536 bits, respectively. Nonetheless, the code rate that is associated to each TBS is fixed, and depends on the values that  $I_{\text{TBS}}$  and  $I_{\text{RU}}$  take. More precisely, the code rate that correspond to a given NB-IoT transmission in uplink is given by

$$R_c^{\text{UL}} = \frac{\text{TBS}}{N_{\text{RE}} N_{\text{RU}} N_{\text{b}}}, \quad (1)$$

where  $N_{\text{RE}}$  is the number of Resource Elements (RE) allocated per RU,  $N_{\text{RU}}$  is the number of RUs utilized in each NB-IoT information block, and  $N_{\text{b}}$  is the number of bits that is transmitted in each resource element. Note that  $N_{\text{RE}} = 96$  (144) for single-tone (multi-tone) transmission, whereas  $N_{\text{b}} = 1$  (2) for BPSK (QPSK) modulation, respectively. In addition, Table 5 shows the number of RUs that fit in each information block as function of the RU index that is selected.

**Table 4.** Number of bits per information block as function of the Transport Block Size index and the Resource Unit index (see Table 16.5.1.2-2 of [3]).

$I_{\text{TBS}}$	$I_{\text{RU}}$							
	0	1	2	3	4	5	6	7
0	16	32	56	88	120	152	208	256
1	24	56	88	144	176	208	256	344
2	32	72	144	176	208	256	328	424
3	40	104	176	208	256	328	440	568
4	56	120	208	256	328	408	552	680
5	72	144	224	328	424	504	680	872
6	88	176	256	392	504	600	808	1000
7	104	224	328	472	584	712	1000	1224
8	120	256	392	536	680	808	1096	1384
9	136	296	456	616	776	936	1256	1544
10	144	328	504	680	872	1000	1384	1736
11	176	376	584	776	1000	1192	1608	2024
12	208	440	680	1000	1128	1352	1800	2280
13	224	488	744	1032	1256	1544	2024	2536

In our simulation setting, the value of TBS was fixed. Then, from Table 4, we obtained the different  $I_{\text{TBS}}$  and  $I_{\text{RU}}$  combinations that can be supported with the selected TBS. Each  $I_{\text{RU}}$  can be associated with the required number of resource units ( $N_{\text{RU}}$ ) taking advantage of Table 5. Note that when  $N_{\text{RU}} = 1$ , then we are in presence of a single-tone transmission, where the number of resource elements

**Table 5.** Number of Resource Units that corresponds to the different Resource Unit indexes of the NPUSCH (see Table 16.5.1.1-2 of [3]).

$I_{RU}$	$N_{RU}$
0	1
1	2
2	3
3	4
4	5
5	6
6	8
7	10

**Table 6.** Code rates for NPUSCH Format 1 in terms of the Transport Block Size and Resource Unit indexes for a single-tone transmission. Code rates are obtained from (1).

Modulation Order	$I_{TBS}$	Index of Resource Units $I_{RU}$ (Single-Tone case)							
		0	1	2	3	4	5	6	7
1	0	0.17	0.17	0.19	0.23	0.25	0.26	0.27	0.27
1	2	0.33	0.38	0.50	0.46	0.43	0.44	0.43	0.44
2	1	0.13	0.15	0.15	0.19	0.18	0.18	0.17	0.18
2	3	0.21	0.27	0.31	0.27	0.27	0.28	0.29	0.30
2	4	0.29	0.31	0.36	0.33	0.34	0.35	0.36	0.35
2	5	0.38	0.38	0.39	0.43	0.44	0.44	0.44	0.45
2	6	0.46	0.46	0.44	0.51	0.53	0.52	0.53	0.52
2	7	0.54	0.58	0.57	0.61	0.61	0.62	0.65	0.64
2	8	0.63	0.67	0.68	0.70	0.71	0.70	0.71	0.72
2	9	0.71	0.77	0.79	0.80	0.81	0.81	0.82	0.80
2	10	0.75	0.85	0.88	0.89	0.91	0.87	0.90	0.90

is  $N_{RE} = 96$ . Otherwise, the transmission is multi-tone, and the number of resource elements is  $N_{RE} = 144$ . Assuming that the value of  $I_{TBS}$  is known, the associated modulation order of the transmission ( $N_b$ ) can be found in Table 3. Finally, Table 6 shows the code rates supported in a single-tone transmission.

For instance, if we set TBS equal to 256 bits, then Table 6 shows the code rates that the NPUSCH Format 1 can support when BPSK and QPSK modulation for different Resource Unit indexes ( $I_{RU}$ ). Therefore, from Table 7, we observe that if

**Table 7.** Code rates for NPUSCH Format 1 in terms of Resource Unit index for a single-tone transmission when the Transport Block Size is set to 256 bits.

Modulation	Index of Resource Units $I_{RU}$ (Single-Tone case)							
	0	1	2	3	4	5	6	7
BPSK	-	-	-	-	-	0.44	-	0.27
QPSK	-	0.67	0.44	0.33	0.27	-	0.17	-

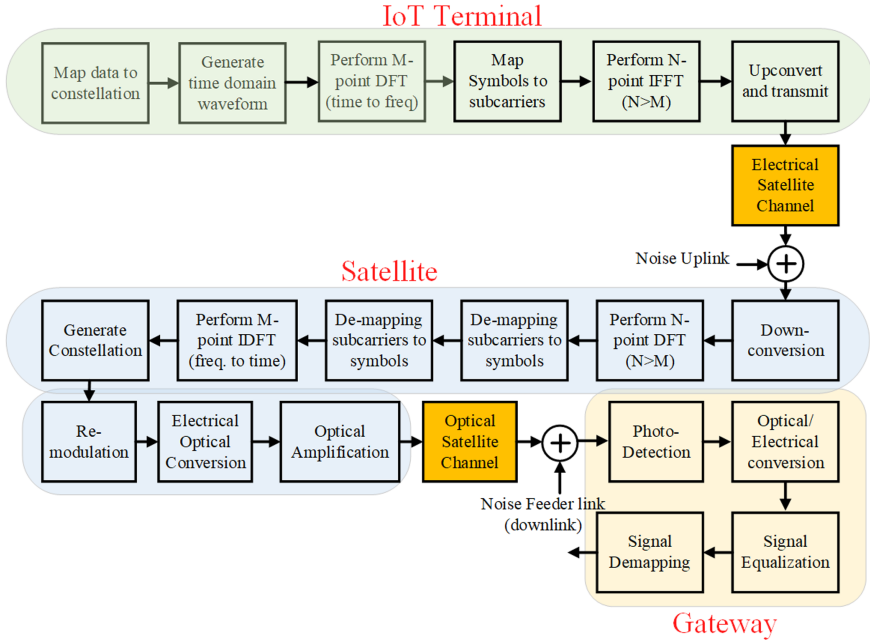


**Fig. 2.** Block diagram of the hybrid radio/optical reverse link of the IoT satellite system. The radio access link starts in the IoT terminal (green blocks) and ends in the GEO satellite (blue blocks). The M-QAM symbols detected onboard the satellite are forwarded in the optical feeder link using a M-PAM constellation. Finally, the IoT payload bits are finally recovered in the satellite gateway after error control decoding (orange blocks). (Color figure online)

the value of TBS is set to 256 bits and  $N_b = 1$  (BPSK modulation), then it is only possible to use two different code rates:  $R_c^{UL} = 0.27$  (with  $I_{RU} = 9$ ) and  $R_c^{UL} = 0.44$  (with  $I_{RU} = 5$ ). On the contrary, for a TBS of 256 bits and  $N_b = 2$  (QPSK modulation), there are five possible code rates:  $R_c^{UL} = 0.17, 0.27, 0.33, 0.44, 0.67$  (with  $I_{RU} = 1, 2, 3, 4, 6$ , respectively). Note that when  $I_{RU} = 0$ , there is no MCS that can be supported for a TBS of 256 bits.

After the encoding and modulation is performed, the uplink NB-IoT symbols are accommodated into a Single-Carrier Frequency Division Multiplex Access (SC-FDMA) waveform, which can be efficiently implemented with the aid of a Discrete Fourier Transform (DFT) pre-processing, just before the Inverse Fast Fourier Transform (IFFT) block. After that, the signal is upconverted and transmitted to the satellite on a suitable Radio Frequency (RF) band. The SC-FDMA signal that is received in the satellite is then demodulated and re-mapped into a single-carrier  $M$ -PAM waveform, which is suitable to vary the intensity of light beam that the laser diode emits in a proportional way to signal's amplitude in downlink. On the other side of optical feeder link, the satellite gateway performs the optical-to-electrical conversion with the aid of a photodetector (direct

detection), where the payload of the IoT transmission is finally recovered after demodulation and decoding the received codeword. For a general overview of the different blocks that constitute the reverse link of the GEO satellite system, please refer to Fig. 2.

## 2.2 Optical Transmission in Feeder Link (Downlink of Reverse Link)

Without loss of generality, the time-domain signal that is used to modulate the intensity of the optical feeder link can be written as

$$s(t) = \sum_k s[k] g_{\text{tx}}(t - k(1 - \delta)T_s), \quad (2)$$

being  $k$  the index of the data symbol in its input vector  $\{s[k]\}$ ,  $T_s$  represents the Nyquist data rate,  $g_{\text{tx}}(t)$  models the response of the pulse-shaping filter in the time domain, and  $\delta$  indicates the overlapping factor used for time-packing. The transmit pulses with response  $g_{\text{tx}}(t)$  are designed to have unit energy and to be orthogonal to the pulses at distances multiple of  $T_s$ . Nevertheless, when implementing time-packing, the orthogonality among adjacent pulses is not verified any more, as  $\int_{-\infty}^{\infty} g_{\text{tx}}(t)g_{\text{tx}}(t - n(1 - \delta)T_s)dt = 0$  only it is satisfied when  $\delta = 0$  (*i.e.*, there is no overlapping among adjacent pulses). By doing so, it is obtained a higher data rate at expenses of introducing ISI. Specifically, the obtained data rate is *i.e.*,

$$R'_s = \frac{R_s}{(1 - \delta)} \geq R_s = \frac{1}{T_s}. \quad (3)$$

Note that the new  $R'_s$  can be attained without enlarging the transmission bandwidth. Thanks to this approach, it can be concluded that time-packing is able to use the communication bandwidth in a more efficient way. The price to pay is the addition of ISI in the transmitted signal, which must be mitigated in reception.

The driving voltage of the external MZM that is placed onboard the satellite for Electrical-to-Optical (E/O) conversion is given by

$$v_{\text{mzm}}(t) = V_B + \beta \tilde{s}(t) (V_\pi/\pi), \quad (4)$$

where  $V_B$  and  $V_\pi$  are the bias and half-wavelength voltages of the MZM,  $\beta$  is the intensity modulation index, and

$$\tilde{s}(t) = s(t)/\sqrt{\mathbb{E}\{|s(t)|^2\}} \quad (5)$$

is the constellation with unity energy. In the latter formula,  $\mathbb{E}\{\cdot\}$  represents the mathematical expectation of the corresponding time-domain signal. There the parameter  $\beta$  determines the MZM's working range. Large  $\beta$  augment the transmitted optical power but also the non-linear distortion the output of the Photodetector (PD) in the satellite gateway. The relationship between the electrical voltage and optical field that provides the MZM is given by [10]

$$E_o(t) = \cos\left(\frac{\pi}{2} \frac{v_{\text{mzm}}(t)}{V_\pi}\right) \sqrt{2P_{o,\text{id}}} \cos(\omega_o t), \quad (6)$$

where  $P_{o,ld}$  is the average optical power of the Laser Diode (LD) that feeds the MZM whereas  $\omega_o$  represents the angular frequency of the transmitted *unmodulated optical carrier* in the *optical sidebands*. Thus, the temporal optical intensity modulated signal at the output of the MZM is

$$\begin{aligned} p_o(t) = E_o^2(t) &= \cos^2\left(\frac{\pi}{2} \frac{v_{mzm}(t)}{V_\pi}\right) 2P_{o,ld} \cos^2(\omega_o t) \\ &= \left[1 + \cos\left(\frac{\pi V_B}{V_\pi} + \beta \tilde{s}(t)\right)\right] P_{o,ld} \cos^2(\omega_o t). \end{aligned} \quad (7)$$

considering that the quadrature bias point is  $V_B = (3V_\pi)/2$ , then,

$$p_o(t) = \left[1 + \sin(\beta \tilde{s}(t))\right] P_{o,ld} \cos^2(\omega_o t) \approx \underbrace{\left[1 + \beta \tilde{s}(t)\right]}_{\text{modulating signal}} \underbrace{P_{o,ld} \cos^2(\omega_o t)}_{\text{optical carrier}} \quad \beta \ll 1, \quad (8)$$

where in previous expression it has been the following approach  $\sin(x) \approx x$  for  $x \ll 1$ . Thus, the impact of the MZM's non-linear effects can be neglected. Next, the optical Free Space Loss (FSL) is

$$L_{o,fsl} = \lambda^2 / (4\pi d_{fso})^2, \quad (9)$$

where  $d_{fso}$  is the link range and  $\lambda$  is the wavelength that the optical feeder link utilizes. Besides the FSL, it is required to take the atmospheric losses, loss  $L_{o,atm}$ , into account. Specially, when there are bad weather conditions.

The optical signal that reaches the PD generates an electrical current, *i.e.*,

$$i_D(t) = I_D + i_d(t) = \mu \frac{G_{o,tx} G_{o,rx} G_{o,edfa}}{L_{o,fsl} L_{o,atm} L_{o,sys}} \int_t^{t+T_o} p_o(\tau) d\tau, \quad (10)$$

$$\int_t^{t+T_o} p_o(\tau) d\tau = \frac{P_{o,ld}}{2} \left[1 + \sin(\beta \tilde{s}(t))\right], \quad (11)$$

being  $T_o = 2\pi/\omega_o$  the optical's carrier period,  $\mu$  [A/W] is the PD responsivity,  $G_{o,tx}$  and  $G_{o,rx}$  represent the optical gains of the transmit and receive telescopes,  $G_{o,edfa}$  identifies the gain of the Erbium-Doped Fiber Amplifier (EDFA) sited before the satellite gateway's PD, and  $L_{o,sys}$  symbolizes the system losses in the optical feeder link. At this point, it is necessary to remark that the current in (10) is decomposed in two components, where the DC component is given by

$$I_D = \mu \frac{G_{o,tx} G_{o,rx} G_{o,edfa}}{L_{o,fsl} L_{o,atm} L_{o,sys}} \frac{P_{o,ld}}{2}, \quad (12)$$

and it is independent of  $\beta$ , whereas the AC component depends on it, and can be equated as

$$i_d(t) = i_D(t) - I_D = I_D \sin(\beta \tilde{s}(t)) \approx I_D \beta \tilde{s}(t) \quad \beta \ll 1. \quad (13)$$

The direct-detected electrical's signal SNR by the satellite gateway's PD is

$$\text{SNR}_{e,pd} = \frac{\mathbb{E}\{|i_d(t)|^2\}}{\mathbb{E}\{|n_o(t)|^2\}} \approx \frac{I_D^2 \beta^2}{\mathbb{E}\{|n_o(t)|^2\}} \quad \beta \ll 1, \quad (14)$$

where

$$\mathbb{E}\{|n_o(t)|^2\} = \mathbb{E}\{|i_{\text{shot}}(t)|^2\} + \mathbb{E}\{|i_{\text{thermal}}(t)|^2\} + \mathbb{E}\{|i_{\text{rin}}(t)|^2\} + \mathbb{E}\{|i_{\text{beat}}(t)|^2\} \quad (15)$$

includes the contribution of all noise sources in the optical feeder link, namely the *shot noise* sources, *thermal noise*, *Relative Intensity Noise* (RIN) of LD, and *beat noise* [7]. Note that shot noise term includes the contribution of the received optical signal, the Amplified Spontaneous Emission (ASE) noise, the background optical noise and the dark current noise, whereas the beat noise term accounts the effect of combining the received optical signal with the ASE noise.

If the received optical power is ranged between  $-90$  and  $-20$  dBW, the beat noise is the dominant one in the optical's feeder link SNR [13]. In this situation,

$$\mathbb{E}\{|n_o(t)|^2\} \approx \mathbb{E}\{|i_{\text{beat}}(t)|^2\} = 4 I_D I_{\text{ase}} (B_e/B_o), \quad (16)$$

where  $B_o$  is the bandwidth of the optical signal at the PD input,  $B_e$  is the bandwidth of the electrical signal at the PD output, and  $I_{\text{ase}} = \mu G_{o,\text{edfa}} P_{\text{ase}}$  is the DC component generated by the ASE noise, whose equivalent noise power at the input of the EDFA (*i.e.*, before amplification) is given by  $P_{\text{ase}} = \rho_{\text{ase}} B_o$ .

Let  $r(t) = s(t) + n(t)$  be the continuous-time received signal, being  $n(t)$  the Additive White Gaussian Noise (AWGN). Then, after applying Matched Filtering (MF) [8], the received signal samples can be written as

$$r[n] = \int_{-\infty}^{\infty} r(t) g_{\text{rx}}(t - n(1 - \delta)T_s) dt = \sum_k s[k] c[k - n] + \eta[n]. \quad (17)$$

Taking into account that  $g_{\text{rx}}(t) = g_{\text{tx}}(-t)^*$ , it is possible to show that

$$c[k - n] = \int_{-\infty}^{\infty} g_{\text{tx}}(t - k(1 - \delta)T_s) g_{\text{tx}}(-t + n(1 - \delta)T_s)^* dt, \quad (18)$$

$$\eta[n] = \int_{-\infty}^{\infty} n(t) g_{\text{tx}}(-t + n(1 - \delta)T_s)^* dt. \quad (19)$$

We note that this is the observation model of Ungerboeck [17]. Unfortunately, the ISI in (17) is non-causal and the noise samples  $\eta[n]$  are correlated. To circumvent these drawbacks, it has been whitened the signal after the MF block [16]. By doing so, we obtain

$$r'[n] = \sum_k s[k] c'[k - n] + \eta'[n], \quad (20)$$

where  $c'[k]$  for  $k \neq n$  is the causal ISI, verifying  $c'[k] * c'[-k]^* = c[k]$ , and  $\eta'[n]$  are AWGN samples. The duration and value of ISI depends on the selected roll-off  $\rho$ , the modulation order  $M$ , and overlapping  $\delta$ .

We now focus on re-writing the received signal samples in (20) in a vector-matrix form. For this, we define  $\mathbf{r}' \in \mathbb{R}^{(N+L_c) \times 1}$  as the vector that stacks the received time-packed samples, *i.e.*,

$$\mathbf{r}' = \left[ r' \left[ \frac{(-L_c + 1)}{2} \right] \cdots r'[n] \cdots r' \left[ N + \frac{(L_c - 1)}{2} \right] \right]^T, \quad (21)$$

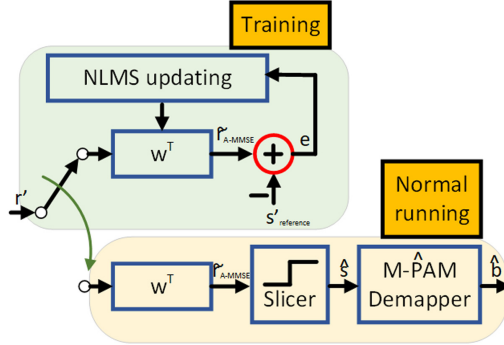


**Fig. 3.** Equalization process using Normalized Least Mean Squares algorithm. Green (orange) blocks illustrate the training (normal) operation phase of the equalizer.

where  $L_c$  is the number of delayed signal samples after the MF, and  $N$  is the number of modulated symbols to-be-transmitted. Then, we can show that

$$\mathbf{r}' = \mathbf{H} \mathbf{s} + \boldsymbol{\eta}', \quad (22)$$

where  $\mathbf{s} \in \mathbb{R}^{(N+(L_c-1)/2) \times 1}$  and  $\boldsymbol{\eta}' \in \mathbb{R}^{(N+L_c) \times 1}$  are the vectors containing the transmitted symbols and the received noise samples, respectively, while  $\mathbf{H} \in \mathbb{R}^{(N+L_c) \times (N+(L_c-1)/2)}$  is the so-called convolution channel matrix. After explaining the key concepts behind time-packing transmission, we are now ready to study the detection strategies to recover the transmitted symbol stream.

### 3 Adaptive Equalization

The most convenient strategy to remove the interference in a multi-path communication channel consist in using the Maximum Likelihood Sequence Estimator (MLSE), whose practical implementation can be notably simplified in a recursive way via the Viterbi Algorithm (VA) [8, 18]. Unfortunately, the trellis diagram that results when implementing the VA in the received sequence of symbol samples has an exponential relationship with the constellation size ( $M$ ) and the channel memory. Note that the channel memory parameter for time-packed signals depends on the pulse-shapping's overlapping ( $\delta$ ) and the roll-off ( $\rho$ ). Thus, the larger is the overlapping factor and/or the lower is the roll-off of factor, the higher is the ISI from time-packing signalling. Unfortunately, using large overlapping factors and low roll-off factors are of high interest, since they permit to increase the throughput of the communication link. Therefore, for these cases, it is not recommended to use VA. Alternatively, we use an adaptive transversal filter that performs linear equalization, as suggested in [4]. By doing so, the received signal sample before performing a symbol-by-symbol detection becomes

$$\hat{s}[n] = \mathbf{w}^T \mathbf{y}[n], \quad (23)$$

where  $\mathbf{w} = [w[0] \cdots w[L_w - 1]]^T$  is the vector that stacks the  $L_w$  weights of the transversal filter, and  $\mathbf{y}[n] = [r'[n - (L_w - 1)/2] \cdots r'[n] \cdots r'[n + (L_w - 1)/2]]^T$  is the vector that stacks the  $(L_w - 1)/2$  *a priori* and *a posteriori* received samples to perform the transmit symbol estimation. To determine the weights of the adaptive linear equalizer, the Normalized Least Mean Squares (NLMS) algorithm is used with the training sequence of symbols that is illustrated in Fig. 3. Then, the updating process of the filter weights for the  $j$ -th Monte-Carlo training sequence at the  $n$ -th training symbol is given by [9]

$$\mathbf{w}_j[n] = \mathbf{w}_j[n - 1] + \frac{\mu}{P_y} e_j[n] \mathbf{y}_j[n], \quad (24)$$

where  $\mathbf{w}_j[n] \in \mathbb{R}^{L_w \times 1}$  and  $\mathbf{w}_j[n - 1] \in \mathbb{R}^{L_w \times 1}$  represent the vector of  $L_w$  coefficients of the transversal filter at the current and previous training iteration, respectively,  $\mu$  is the forgetting factor of the NLMS algorithm,  $P_y$  represents the power of the received signal,  $e_j[n] = s_j[n] - \hat{s}_j[n]$  equates the error from the current estimated symbol and the training one, which are equated as  $\hat{s}_j[n]$  and  $s_j[n]$ .

## 4 Performance Evaluation

The error correction capabilities that the MCS of the NB-IoT standard has on the *end-to-end* reverse link of the GEO satellite system (*i.e.*, from the IoT devices to the satellite gateway) is now evaluated. For this purpose, we first present the simulation setup and, after that, we show the different computed figures of merit that are relevant to characterize the end-to-end error correction performance.

### 4.1 Simulation Setup

The NB-IoT transmitted signal corresponds to the NPUSCH Format 1, assuming that TBS = 256 bits in all cases. The corresponding simulated code rates are:

- $R_c^{\text{UL}} = 0.27, 0.44$  for BPSK (2-PAM) in the radio access (optical feeder) link.
- $R_c^{\text{UL}} = 0.17, 0.67$  for QPSK (4-PAM) in the radio access (optical feeder) link.

The BPSK (QPSK) modulation symbols that the satellite receives in uplink from the IoT terminal are first detected and then re-modulated, using for this purpose a 2-PAM (4-PAM) constellation with a SRRC pulse shaping filter with roll-off factor  $\rho = 0.25$  and overlapping factor  $\delta = \{0, 25, 40\}\%$ . The resulting time-domain signal is used to modulate in intensity the light beam that the LD onboard the satellite generates, using for this purpose an external MZM that works in its linear region. Finally, the optical signal that the satellite gateway receives in downlink is amplified, converted into an electrical signal using a PIN-diode Photodetector (Direct Detection), matched-filtered with the transmit SRRC pulse shape, equalized using an adaptive linear MMSE filter, and turbo decoded.

**Table 8.** Parameters of the optical feeder link used in the NB-IoT satellite system.

Symbol	Optical Link Parameter	Value	Unit
$P_{o,ld}$	Optical power of LD (incl. EDFA booster)	23.0	dBm
$G_{o,tx}$	Optical gain of transmitter (satellite telescope)	114.3	dBi
$G_{o,rx}$	Optical gain of receiver (ground telescope)	125.8	dBi
$L_{o,fsl}$	FSL of optical link (1550 nm, 39000 km)	290.0	dB
$L_{o,atm}$	Atmospheric attenuation	1.7	dB
$L_{o,sys}$	System losses in the optical feeder link	6.5	dB
$G_{edfa}$	Gain of the optical amplifier (EDFA)	50.0	dB
$\mu$	Responsivity of photodetector (PIN diode)	0.5	A/W
$B_e$	Bandwidth of electrical filter (PD output)	1.5	GHz
$B_o$	Bandwidth of optical channel (1550 nm)	12.5	GHz
$\rho_{ase}$	PSD of amplified spontaneous emissions	$2.0 \times 10^{-19}$	W/Hz
$\rho_{rin}$	PSD of RIN process (normalized)	-160	dBc/Hz
$\rho_{back}$	PSD of background noise at EDFA input	$7.6 \times 10^{-25}$	W/Hz
$i_n$	Electrical noise current spectral density	$1.0 \times 10^{-11}$	A
$i_{dark}$	Dark current at the PIN diode output	$1.0 \times 10^{-10}$	A

Table 8 shows the optical feeder link parameters, taking both the optical gains and losses, and the sources of optical noise [13] into account. The effect of any other parameter not listed in this table is considered negligible. From Table 8 it is observed that the average received optical power is formulated as

$$P_{o,rx}[\text{dBm}] = P_{o,ld}[\text{dBm}] + G_{o,tx}[\text{dB}] + G_{o,rx}[\text{dB}] - L_{o,fsl}[\text{dB}] - L_{o,sys}[\text{dB}] - L_{o,atm}[\text{dB}] = -33.4[\text{dBm}] - L_{o,atm}[\text{dB}]. \quad (25)$$

When  $L_{o,atm} = 0$  dB (*i.e.*, clear-sky conditions), the DC current at the PD output is  $I_D = 11.43$  mA, whereas the DC current from the ASE noise is  $I_{ase} = 0.125$  mA regardless of the weather. Thus, if  $\beta = 0.5$ , the PD's output electrical SNR becomes

$$\text{SNR}_{e,pd}[\text{dB}] = 16.75[\text{dB}] - L_{o,atm}[\text{dB}]. \quad (26)$$

The larger is the intensity modulation index  $\beta$ , the more notable becomes the non-linear distortion introduced by the MZM. In this situation, Digital Pre-Distortion (DPD) is needed to keep non-linear distortion under control [7].

The minimum and maximum  $E_b/N_0$  values that were tested in the access link were  $E_b/N_{0_{\min}} = 0$  dB and  $E_b/N_{0_{\max}} = 11$  dB, respectively, with a fixed step size of 0.1 dB. Finally, the SNR for the feeder link was set to  $\text{SNR}_f = 15$  dB for all performance evaluations, according to the parameters listed in Table 8.

**Table 9.** Maximum throughput in the hybrid radio/optical NB-IoT satellite link.

Modulation	Rc=0.27	Rc=0.44	Rc=0.17	Rc=0.67
BPSK	$\delta=0\% \Rightarrow \gamma=0.216$	$\delta=0\% \Rightarrow \gamma=0.352$	-	-
	$\delta=25\% \Rightarrow \gamma=0.288$	$\delta=25\% \Rightarrow \gamma=0.469$		
	$\delta=40\% \Rightarrow \gamma=0.36$	$\delta=40\% \Rightarrow \gamma=0.58$		
QPSK	-	-	$\delta=0\% \Rightarrow \gamma=0.17$	$\delta=0\% \Rightarrow \gamma=1.072$
			$\delta=25\% \Rightarrow \gamma=0.362$	$\delta=25\% \Rightarrow \gamma=1.4293$
			$\delta=40\% \Rightarrow \gamma=0.4533$	$\delta=40\% \Rightarrow \gamma=1.7867$

Thus, we can now show the effect that the optical feeder link transmission (downlink) has in the end-to-end BER, Packet Error Rate (PER) and normalized Throughput. Furthermore, for the uncoded case ( $R_c = 1$ ), we also visualize the upper bound performance for the end-to-end BER, PER and Throughput, which would be achievable in case of an ideal optical feeder link ( $\text{SNR}_{e,\text{pd}} \gg 1$ ), *i.e.*,

$$P_{b,\text{BPSK}} = \frac{1}{2} \text{erfc} \left( \sqrt{\frac{E_b}{N_0}} \right), \quad (27)$$

$$P_{b,\text{QPSK}} = \frac{1}{2} \text{erfc} \left( \sqrt{\frac{E_b}{N_0}} \right) \left[ 1 - \frac{1}{4} \text{erfc} \left( \sqrt{\frac{E_b}{N_0}} \right) \right] \quad (28)$$

Then,  $\text{PER} = 1 - (1 - P_b)^N$ , where  $N$  is the length of the data sequence to transmit, and  $P_b$  is the BER of the access link in case of BPSK/QPSK (here, good enough SNR in the optical feeder link was assumed). Regarding the normalized throughput, it is equal to

$$\text{TP} = \frac{(1 - \text{PER}) N_b R_c}{(1 + \rho)(1 - \delta)}, \quad (29)$$

where  $N_b$  is the number of bits per modulated symbol. Note that the roll-off factor ( $\rho$ ) of the optical feeder link and the code rate  $R_c$  of the NB-IoT transmission penalize the throughput of the end-to-end link, whereas the overlapping factor ( $\delta$ ) and the modulation order ( $N_b$ ) increase it.

The use of time-packing compensates in part the reduction in the data rate that the use of error control coding and finite-duration SRRC pulses introduce. Moreover, the selection of suitable MCS in the end-to-end NB-IoT transmission controls the errors that are added either in the radio access and optical feeder links of the reverse GEO satellite channel. In this regards, Table 9 shows the maximum throughput that is achievable when  $R_c = 0.27, 0.44$  ( $R_c = 0.17, 0.67$ ) with BPSK/2-PAM (QPSK/4-PAM) are used in the access/feeder link, with overlapping factors  $\delta = 0, 25, 40\%$ . This maximum throughput attains the form  $\gamma = \frac{N_b R_c}{(1 + \rho)(1 - \delta)}$ . Finally, the receive equalizer relies on an adaptive linear MMSE filter, as described in Sect. 3, with a 100 000-symbol training,  $L_w = 13$  coefficients to estimate the current symbol, and forgetting factor  $\mu = 0.05$ .

## 4.2 Simulation Results

Figure 4 shows the BER of the reverse link (end-to-end) in terms of the  $E_b/N_0$ . It is composed of three sub-figures, each of them for a different overlapping factor:  $\delta = 0\%$  (Fig. 4a),  $\delta = 25\%$  (Fig. 4b), and  $\delta = 40\%$  (Fig. 4c). In these figures, the modulation is not the essential parameter, but rather the code rate, as the Energy-per-Bit is kept constant for all tested schemes. Consequently, we should expect that the lower is the code rate, the better is the BER. However, this conclusion is valid at high  $E_b/N_0$ , since the redundancy that introduces the channel coding may increase the number of erroneous bits after its iterative decoding process at lower values of  $E_b/N_0$ . As a result, we are able to distinguish three regions in Fig. 4: i) low  $E_b/N_0$  values ( $E_b/N_0 \leq 5$  dB), ii) Medium  $E_b/N_0$  values ( $5$  dB  $\leq E_b/N_0 \leq 7.5$  dB), and iii) High  $E_b/N_0$  values ( $E_b/N_0 \geq 7.5$  dB). In the first region, the scheme with best BER uses QPSK/4-PAM in the access/feeder link with  $R_c = 1$ . This means that the best option at low SNR is an uncoded transmission, since the turbo decoding process augments the number of errors when it is used at lower code rates (*i.e.*, diverges). Next, in the Medium SNR

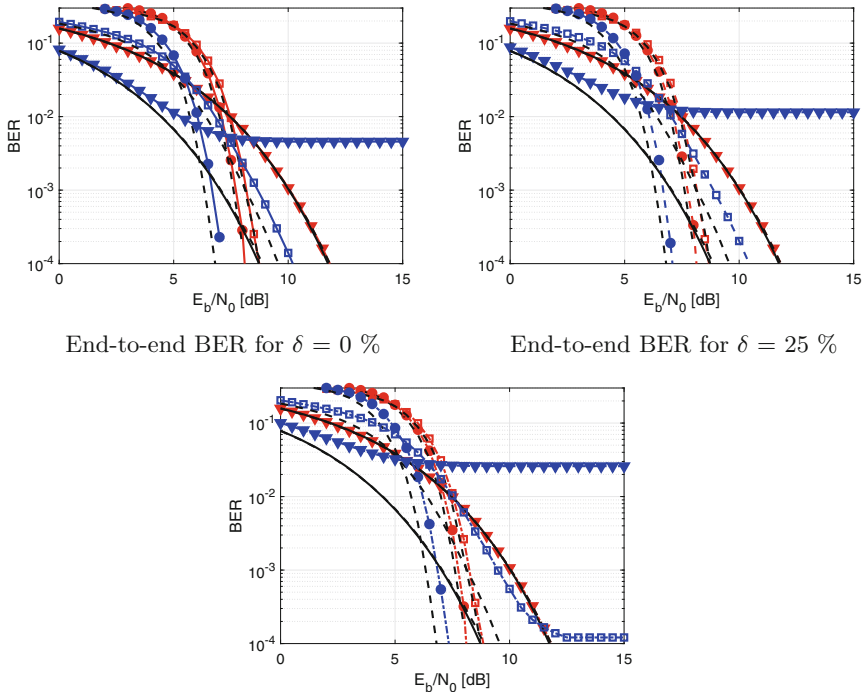


**Fig. 4.** End-to-end BER as a function of  $E_b/N_0$  when  $\rho = 0.25$ . Modulation schemes: BPSK/2-PAM (red lines), QPSK/4-PAM (blue lines). Coded rates:  $R_c = 0.27$  (solid circle markers),  $R_c = 0.44$  (non-filled square markers),  $R_c = 0.17$  (solid diamond markers), and  $R_c = 0.67$  (non-filled triangle markers). Ideal feeder link: Black lines. An adaptive linear MMSE equalizer is used in reception at the satellite gateway.

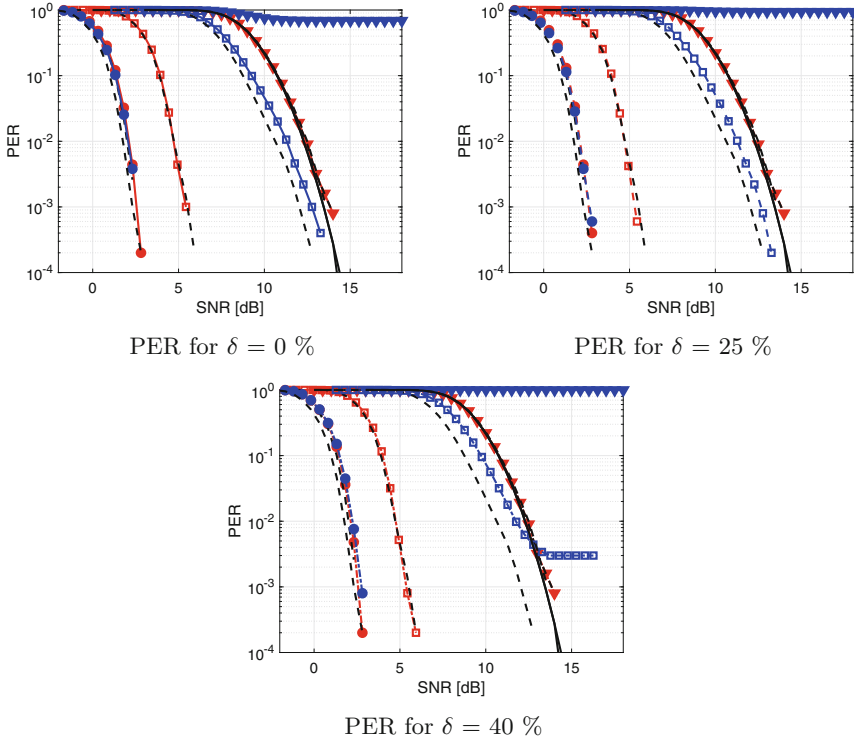


**Fig. 5.** End-to-end PER as a function of SNR when  $\rho = 0.25$ . Modulation schemes: BPSK/2-PAM (red lines), QPSK/4-PAM (blue lines). Overlapping factors:  $\delta = 0$  (continuous lines),  $\delta = 0.25$  (dashed lines), and  $\delta = 0.4$  (dash-dotted lines). Coded rates:  $R_c = 0.27$  (solid circle markers),  $R_c = 0.44$  (non-filled square markers),  $R_c = 0.17$  (solid diamond markers), and  $R_c = 0.67$  (non-filled triangle markers). Ideal feeder link: Black lines. An adaptive linear MMSE equalizer is assumed in reception.

region, the MCS with  $R_c = 0.27$  and  $R_c = 0.44$  start to provide a better BER than the MCS with  $R_c = 0.67$  (the largest one). This means that for these code rates, the turbo-decoded words have a lower number of errors than the received ones. Finally, if the  $E_b/N_0$  is larger than 7.5 dB, then the scheme with lowest code rate provides the best BER performance as it was initially expected.

Regarding the effect of the overlapping factor, we observe that the BER for time-packed BPSK provides very similar performance when compared to the one of BPSK without time-packing. On the contrary, for QPSK modulation and code rate  $R_c = 1$  (uncoded transmission), there is a visible error floor when the SNR of the feeder link is 15 dB at overlapping factors  $\delta = 25\%$  and  $40\%$ . This error floor disappears when the SNR of the feeder link increases. So, the turbo-code permits to reduce/remove the time-packed ISI that the equalizer cannot remove.

Next, Fig. 5 shows the end-to-end PER of the reverse link as function of the SNR of the access link. Similarly, it contains three subfigures, each of them with

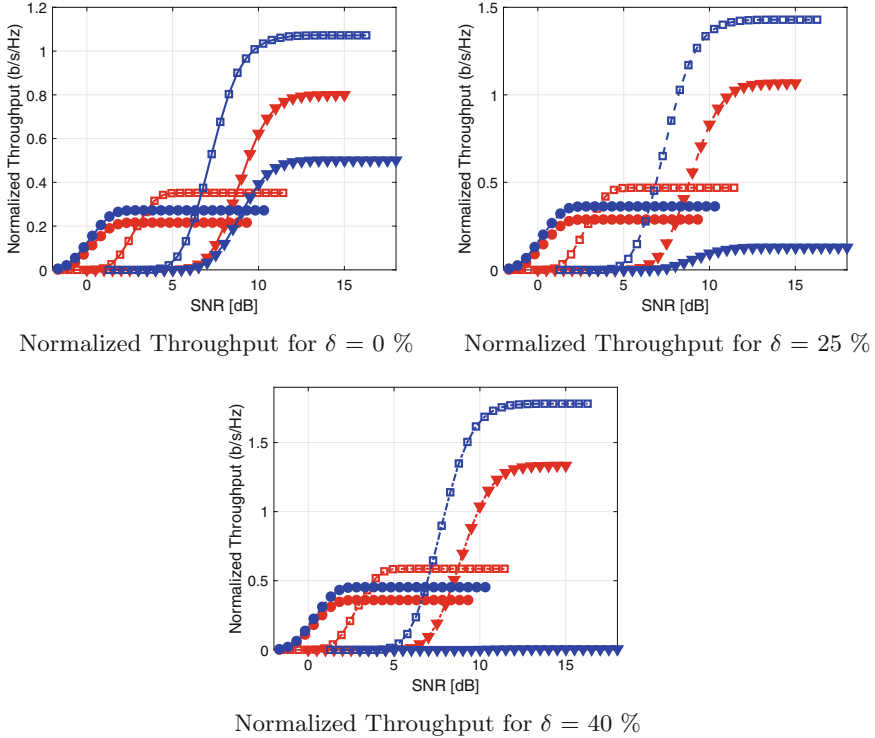


**Fig. 6.** Normalized throughput as a function of SNR when roll-off factor is  $\rho = 0.25$ . Modulation schemes: BPSK/2-PAM (red lines), QPSK/4-PAM (blue lines). Overlapping factors:  $\delta = 0$  (continuous lines),  $\delta = 0.25$  (dashed lines), and  $\delta = 0.4$  (dashed-dotted lines). Code Rates: BPSK/2-PAM  $R_c = 0.27$  (solid circle markers) and  $R_c = 0.44$  (non-filled square markers); QPSK/4-PAM  $R_c = 0.17$  (solid diamond markers) and  $R_c = 0.67$  (non-filled triangle markers). Equalizer used in detection: adaptive MMSE.

a different overlapping factor:  $\delta = 0\%$  (Fig. 5a),  $\delta = 25\%$  (Fig. 5b), and  $\delta = 40\%$  (Fig. 5c). In this case, the distribution of the plotted curves is quite different from Fig. 4, and we observe the lower is the code rate for the given modulation, the better is the PER performance. In this case, it is possible to check that QPSK with  $R_c = 0.17$  and BPSK with  $R_c = 0.27$  provide the best results. Next, it comes the BPSK with  $R_c = 0.44$  and QPSK with  $R_c = 0.67$ . In both cases, PER performance with and without time-packing shows similar performance results. Finally, the uncoded transmissions ( $R_c = 1$ ) provide the worst PER. In fact, all cases with and without time-packing show an error floor. Moreover, the theoretical PER is close to the optimal one for BPSK/QPSK in part of this bound. On the contrary, coded transmissions with(out) time-packing do not show any error floor when the SNR of the feeder link is 15 dB. Furthermore, their performance is close to the one when the feeder link SNR is good enough.

Finally, Fig. 6 shows the normalized throughput in terms of the SNR for overlapping factors  $\delta = 0\%$  (Fig. 6a),  $\delta = 25\%$  (Fig. 6b) and  $\delta = 40\%$  (Fig. 6c). When studying these figures, it is possible to divide them into three regions: i) SNRs lower than 4 dB, ii) SNRs between 4 and 6 dB, and iii) SNRs larger than 6 dB. In the first region, the scheme that provides the best normalized throughput is the one using QPSK/4-PAM modulation and code rate  $R_c = 0.17$ . In the second region, the best scheme uses BPSK/2-PAM modulation and code rate  $R_c = 0.27$ . Finally, in the third region, the scheme that has the largest normalized throughput is the one that uses QPSK/4-PAM modulation with code rate  $R_c = 0.67$ . This classification is independent of using time-packing or not. In all of them, the same distribution is observed. Note that when time-packing is used, a larger normalized throughput is obtained without penalty on the cut-off SNR. This is because the turbo-decoder is able to remove the residual ISI-plus-noise power that the adaptive linear MMSE equalizer is not able to eliminate.

## 5 Conclusions

This paper studied the use of time-packing in the feeder link of a NB-IoT satellite system, which relied on optical wireless technology to implement the downlink transmission from the satellite to the gateway. Performance evaluation was carried out using the BER, PER and Throughput of NPUSCH Format 1 of NB-IoT standard, considering both BPSK or QPSK modulations. The procedure to obtain the code rate that corresponds to the different configurations of the NPUSCH of NB-IoT standard was described, assuming that the Transport Block Size was 256 bits regardless the modulation. It was also assumed that the GEO satellite implemented a Detect-and-Forward strategy, performing a symbol-by-symbol detection, QAM-to-PAM symbol-mapping, time-packing processing, electrical-to-optical conversion, and downlink transmission to the satellite gateway. Finally, an adaptive-MMSE equalizer was assumed in reception at the gateway, in order to mitigate the ISI introduced by time-packing. Simulation results showed that this adaptive-MMSE equalizer was able to remove most of the ISI, leaving aside just a minimal residual part. It was also possible to see that the lower is the SNR of the optical feeder link and/or the higher is the modulation order of the NB-IoT transmission, the worse is the capability of the adaptive-MMSE equalizer to remove the ISI. It was also observed that uncoded BPSK/2-PAM transmissions did not present any error floor at practical optical feeder link SNR values ( $\text{SNR}_{fl} = 15$  dB) and medium/large overlapping factors ( $\delta = 25$  and  $40\%$ ). However, this is not the case for uncoded QPSK/4-PAM modulation, which showed an error floor in the same SNR range. To remove this residual ISI, this paper took advantage of the turbo-decoding process that NB-IoT receivers perform. Simulation results showed that most residual ISI power can be eliminated in reception, even for moderate SNR values in the optical feeder link and large overlapping factors. Consequently, it is possible to conclude that wireless optical links assisted by time-packed waveforms represent an interesting solution for extending the data rates Beyond 5G, particularly in

integrated terrestrial-satellite networks. This claim becomes more relevant in IoT services, whose traffic demand will notably increase in the next few years.

## References

1. 3GPP: LTE; Evolved universal terrestrial radio access (E-UTRA); Multiplexing and channel coding. 3GPP tech. specification, TS 36.212, Ver. 15.9 Rel. 15 (2018)
2. 3GPP: LTE; Evolved universal terrestrial radio access (E-UTRA); Physical channels and modulation. 3GPP tech. specification, TS 36.211, Ver. 15.2 Rel. 15 (2018)
3. 3GPP: LTE; Evolved universal terrestrial radio access (E-UTRA); Physical layer procedures. 3GPP tech. specification, TS 36.213, Ver. 15.9 Rel. 15 (2018)
4. Bas, J., Dowhuszko, A.: Linear time-packing detectors for optical feeder link in high throughput satellite systems. In: Proceedings of 1st Mosharaka International Conference on Emerging Applications of Electrical Engineering, pp. 1–6, September 2020
5. Bas, J., Dowhuszko, A.: Time-packing as enabler of optical feeder link adaptation in high throughput satellite systems. In: Proceedings of 5G World Forum, pp. 1–7, September 2020
6. Bas, J., Pérez-Neira, A.: On the physical layer security of IoT devices over satellite. In: Proceedings of European Signal Processing Conference, pp. 1–5, September 2019
7. Dowhuszko, A., Mengali, A., Arapoglou, P., Pérez-Neira, A.: Total degradation of a DVB-S2 satellite system with analog transparent optical feeder link. In: Proceedings of IEEE Global Communications Conference, pp. 1–6, December 2019
8. Forney, G.: Maximum-likelihood sequence estimation of digital sequences in the presence of intersymbol interference. *IEEE Trans. Inform. Theory* **18**(3), 363–378 (1972)
9. Haykin, S.: *Adaptive Filter Theory: International Edition*. Pearson Education Limited, London (2014)
10. Leibrich, J., Ali, A., Paul, H., Rosenkranz, W., Kammeyer, K.: Impact of modulator bias on the OSNR requirement of direct-detection optical OFDM. *IEEE Photonics Technol. Lett.* **21**(15), 1033–1035 (2009)
11. London School of Economics: *Nanosatellite telecommunications: A market study for IoT/M2M applications*, August 2017
12. Mazo, J.: Faster-than-Nyquist signaling. *Bell Syst. Tech. J.* **54**, 1451–1462 (1975)
13. Mengali, A.: *Optical feeder link satellite systems*. In: *Link Optimization in future generation satellite systems*, chap. 4, pp. 61–86. Ph.D. thesis, University of Luxembourg, October 2018
14. Modenini, A.: *Advanced transceivers for spectrally efficient communications*. Ph.D. dissertation, January 2014
15. Northern Sky Research: *M2M and IoT via satellite 10*, December 2019
16. Rusek, F., Anderson, J.: Constrained capacities for Faster-than-Nyquist signaling. *IEEE Trans. Inform. Theory* **55**(2), 764–775 (2009)
17. Ungerboeck, G.: Adaptive maximum-likelihood receiver for carrier-modulated data-transmission systems. *IEEE Trans. Commun.* **22**(5), 624–636 (1974)
18. Viterbi, A.: Error bounds for convolutional codes and an asymptotically optimum decoding algorithm. *IEEE Trans. Inform. Theory* **13**(2), 260–269 (1967)